The elastodynamic response of a semi-infinite anisotropic solid to sudden surface loading

A. G. Every, K. Y. Kim and A. A. Maznev

Citation: The Journal of the Acoustical Society of America **102**, 1346 (1997); doi: 10.1121/1.420053
View online: https://doi.org/10.1121/1.420053
View Table of Contents: https://asa.scitation.org/toc/jas/102/3
Published by the Acoustical Society of America

ARTICLES YOU MAY BE INTERESTED IN

Time domain dynamic response functions of elastically anisotropic solids
The Journal of the Acoustical Society of America **95**, 2505 (1994); https://doi.org/10.1121/1.409860

Dynamic surface acoustic response to a thermal expansion source on an anisotropic half space
The Journal of the Acoustical Society of America **133**, 2634 (2013); https://doi.org/10.1121/1.4799019

Phase-controlled, heterodyne laser-induced transient grating measurements of thermal transport properties in opaque material
Journal of Applied Physics **111**, 023503 (2012); https://doi.org/10.1063/1.3675467

Nanoscale thermal transport
Journal of Applied Physics **93**, 793 (2003); https://doi.org/10.1063/1.1524305

Single crystal elastic constants evaluated with surface acoustic waves generated and detected by lasers within polycrystalline steel samples
Journal of Applied Physics **119**, 043103 (2016); https://doi.org/10.1063/1.4940367

Time-resolved, dual heterodyne phase collection transient grating spectroscopy
Applied Physics Letters **110**, 211106 (2017); https://doi.org/10.1063/1.4983716

ASA

Advance your science and career as a member of the
ACOUSTICAL SOCIETY OF AMERICA

LEARN MORE

The elastodynamic response of a semi-infinite anisotropic solid to sudden surface loading

A. G. Every, K. Y. Kim,[a] and A. A. Maznev[b]
University of the Witwatersrand, PO WITS 2050, South Africa

(Received 5 December 1996; accepted for publication 28 April 1997)

Integral expressions are derived for the displacement response tensor of a semi-infinite anisotropic elastic continuum of unrestricted symmetry to a concentrated force suddenly applied to its surface. The surface response is reduced to a one-dimensional integral for numerical evaluation, while the interior response is left as a two-dimensional integral. Calculated surface response functions for Cu(001) are presented. These display multiple Rayleigh wave arrival singularities as well as bulk wave arrivals. Calculated interior response functions for Zn(0001) are presented. These display bulk and head wave arrivals. In followup papers these methods will be used in the interpretation of capillary fracture generated waveforms measured in a number of different materials. © *1997 Acoustical Society of America.* [S0001-4966(97)06208-5]

PACS numbers: 43.20.Gp [ANN]

INTRODUCTION

There is growing interest in the dynamic response functions (Green's functions) of elastically anisotropic solids.[1–14] Part of the reason for this is the need for simple and efficient computational algorithms for use in interpreting waveform data emanating from laser ultrasound experiments,[15–18] transmission and reflection acoustic microscopy,[19–22] and various other transient wave experiments.[23,24] For some purposes it is sufficient to trace the progress of wave arrivals through the medium, making use of the ray approximation.[15–17] In some cases detailed transmission waveforms measured in samples of finite geometry can be reasonably well accounted for with response functions calculated for the infinite continuum.[1] Surfaces do, however, have a modifying effect on transmission waveforms, and this generally becomes more pronounced as the sensing point is moved away from epicenter and head waves come into prominence.[25] When the displacement is measured on the same surface as the applied force, the surface plays a determining role in the response, which tends to be dominated by one or more Rayleigh wave or pseudo-surface-wave arrivals.

This paper is the first in a three part series in which we show that surface and also to a large extent transmission waveforms, generated by a transient force acting on the surface of an elastically anisotropic solid, conform well to dynamic response functions calculated for the semi-infinite continuum. Reverberation effects arising from reflections from the opposite faces and sidewalls lie outside the scope of the present series of articles.

The problem of the displacement response of an elastic half-space to a point or line load suddenly applied at the surface has received wide attention over the years, since first being posed by Lamb.[26] Analytical solutions for point and line loading of an isotropic half-space were first obtained by Cagniard by a method involving Laplace transformation and intricate deformation of the integration contour to analytically perform one of the integrations in the inverse transformation. These celebrated solutions are to be found in a number of books on the dynamics of solids.[27,28] Burridge[29] extended the Cagniard method to calculate the response of an anisotropic half space to an impulsive line load at the surface, and similar results have been obtained through direct integration by Maznev and Every.[30] The Cagniard–de Hoop method has been extensively reviewed by van der Hijden.[31] Willis[32] in a seminal paper obtained the formal solutions to a wide class of self similar problems for the anisotropic half-space using Fourier and radon transforms, and this method has been further developed by Wang and Achenbach.[4] Payton[33] has treated a number of problems for transversely isotropic half-spaces that admit closed-form solutions. Recently Mourad *et al.*[5] have used the Cagniard–de Hoop method to calculate the interior response of anisotropic half spaces of hexagonal and cubic symmetry to point loading. Their method reduces ultimately to a single angular integral which has to be done numerically. Another approach that has been taken recently in calculating response functions of anisotropic half spaces is integral representation in terms of a δ function by Tewary and Fortunko.[13,14]

In this paper we establish methods for calculating the dynamic response at surface and interior points of a semi-infinite anisotropic elastic continuum of unrestricted symmetry to a point load suddenly applied at the surface. Our approach is to Fourier transform the equations of motion and boundary conditions with respect to time and the spatial coordinates parallel to the surface, solve the resulting algebraic equations, and then carry out the inverse transformation. The surface response is reduced to a one-dimensional integral for numerical evaluation, while the interior response is left as a two-dimensional integral. The method we use for computing these numerical integrals is able to cope with Rayleigh poles and pseudo-surface-wave resonances. Our method of calculating the interior response, in that it is in the form of a two dimensional integral, is computationally somewhat less efficient than the Cagniard–de Hoop method[5] and the method of

[a]Present address: Department of Theoretical and Applied Mechanics, Cornell University, Ithaca, NY 14853.
[b]Present address: Department of Chemistry, MIT, Cambridge, MA 02139.

Wang and Achenbach,[4] but it has the advantage of conceptual simplicity and ease of implementation. In our analysis we give particular attention to wave arrival singularities, which are a striking feature of both surface and interior responses. By way of illustrative numerical example, we present calculated surface responses for Cu(001) and interior responses for Zn(0001). In subsequent papers in this series, we apply our method to the interpretation of capillary fracture generated surface and transmission waveforms in a number of different materials.

I. METHOD OF CALCULATION

We consider a general anisotropic elastic continuum of density ρ and elastic modulus tensor C_{ijkl} occupying the half-space $x_3>0$. A concentrated point force $\mathbf{F}(t)=(F_j\epsilon(t))$ with sign-function time dependence

$$\epsilon(t)=\begin{cases}1, & t>0\\ -1, & t<0\end{cases} \tag{1}$$

acts at the origin on the otherwise free surface of the half-space. The displacement field $\mathbf{u}(\mathbf{x},t)$ in response to this force is given by

$$u_i(\mathbf{x},t)=G_{ij}^{\epsilon}(\mathbf{x},t)F_j, \tag{2}$$

where $G_{ij}^{\epsilon}(\mathbf{x},t)$ is the response function tensor.

Later in this paper we shift our attention to the response function $G_{ij}^{\Theta}(\mathbf{x},t)$ pertaining to a force with Heaviside step function time dependence

$$\Theta(t)=\tfrac{1}{2}\{\epsilon(t)+1\}, \tag{3}$$

which is more amenable to direct measurement. Rather than calculating $G_{ij}^{\Theta}(\mathbf{x},t)$ directly, it is somewhat simpler to calculate $G_{ij}^{\epsilon}(\mathbf{x},t)$ and then obtain $G_{ij}^{\Theta}(\mathbf{x},t)$ from

$$G_{ij}^{\Theta}(\mathbf{x},t)=\tfrac{1}{2}\{G_{ij}^{\epsilon}(\mathbf{x},t)-G_{ij}^{\epsilon}(\mathbf{x},0)\}. \tag{4}$$

This sidesteps the δ function that occurs in the Fourier transform of $\Theta(t)$, but not that of $\epsilon(t)$. The time derivative of $G_{ij}^{\Theta}(\mathbf{x},t)$ is the dynamic Green's tensor of the medium.

The displacement field is required to satisfy the equations of motion

$$\rho\frac{\partial^2 u_i}{\partial t^2}=C_{ijkl}\frac{\partial^2 u_l}{\partial x_j\,\partial x_k}, \quad x_3>0, \tag{5}$$

subject to the boundary conditions on the stress tensor

$$\sigma_{\not\parallel 3}(\mathbf{x}_\parallel,x_3=0_+,t)=-F_j\delta_{jl}\delta(\mathbf{x}_\parallel)\epsilon(t), \tag{6}$$

where $\mathbf{x}_\parallel=(x_1,x_2)$ denotes the position vector in the surface and $\delta(\mathbf{x}_\parallel)=\delta(x_1)\,\delta(x_2)$ is the two-dimensional δ function. The negative sign in Eq. (6) arises from the fact that the surface tractions $\sigma_{j3}(\mathbf{x}_\parallel,x_3=0_+,t)$ are in reaction to the applied force. The initial conditions are $G_{ij}^{\Theta}(\mathbf{x},t)=0,\ t<0$.

Representing the boundary conditions in terms of their Fourier transform with respect to $\mathbf{x}_\parallel$ and t, we have

$$\sigma_{l3}(\mathbf{x}_\parallel,x_3=0_+,t)=\int_{-\infty}^{\infty}d^2k_\parallel\int_{-\infty}^{\infty}d\omega\,\frac{F_j\delta_{jl}}{4\pi^3 i\omega}\times\exp\{i(\mathbf{k}_\parallel.\mathbf{x}_\parallel-\omega t)\}, \tag{7}$$

where $\mathbf{k}_\parallel=(k_1,k_2)$ is the projection of the wave vector in the surface and ω is the angular frequency.

We seek a solution to the equations of motion (5) and boundary conditions (7) in the form of a superposition of outgoing plane waves whose amplitudes are proportional to F_j:

$$u_i(\mathbf{x},t)=\int_{-\infty}^{\infty}d^2k_\parallel\int_{-\infty}^{\infty}d\omega\sum_{n=1}^{3}A_j^{(n)}F_jU_i^{(n)}\times\exp\{i(\mathbf{k}_\parallel\cdot\mathbf{x}_\parallel+k_3^{(n)}x_3-\omega t)\}. \tag{8}$$

For each value of $\mathbf{k}_\parallel$ and ω, the third component k_3 of $\mathbf{k}$ and the polarization vector $\mathbf{U}$ are related by the Christoffel equations

$$(C_{ijkl}s_js_k-\rho\delta_{il})U_l=0, \tag{9}$$

where $\mathbf{s}=\mathbf{k}/\omega$, is the acoustic slowness vector and $s_3^{(n)}$are roots of the characteristic sextic equation

$$\det|C_{ijkl}s_js_k-\rho\delta_{il}|=0. \tag{10}$$

Equation (10) yields six solutions of which three are chosen which correspond to outgoing waves, on the basis that they are either homogeneous (bulk) waves with ray vectors directed into the interior, or inhomogeneous (evanescent) waves which decay into the interior.[34] The choice of outgoing waves depends on the sign of ω, which will be restricted to positive values, as explained later.

From the stress–strain relationship, $\sigma_{lm}=C_{lmpq}\partial u_p/\partial x_q$, and Eq. (8) it follows that the surface tractions are given by

$$\sigma_{l3}(\mathbf{x}_\parallel,x_3=0_+,t)=\int_{-\infty}^{\infty}d^2k_\parallel\int_{-\infty}^{\infty}d\omega\ i\omega\sum_{n=1}^{3}A_j^{(n)}F_jB_l^{(n)}\times\exp\{i(\mathbf{k}_\parallel\cdot\mathbf{x}_\parallel-\omega t)\}, \tag{11}$$

where

$$B_l^{(n)}=\sum_{pq}C_{3lpq}U_p^{(n)}s_q^{(n)}, \tag{12}$$

in which $(s_1^{(n)},s_2^{(n)})=(s_1,s_2)$. Comparing (7) and (11) we arrive at a set of three linear equations for the partial wave weighting factors $A_j^{(n)}$

$$\sum_{n=1}^{3}A_j^{(n)}B_l^{(n)}=-\delta_{jl}/4\pi^3\omega^2. \tag{13}$$

These have solution

$$A_j^{(n)}=-\frac{1}{4\pi^3\omega^2}(\mathbf{B}^{-1})_j^{(n)}=-\frac{1}{4\pi^3\omega^2}\frac{\mathrm{adj}(\mathbf{B})_j^{(n)}}{\det|\mathbf{B}|}, \tag{14}$$

adj denoting matrix adjoint.

From Eqs. (2), (8), and (14) it follows that

$$G_{ij}^{\epsilon}(\mathbf{x},t)=-\frac{1}{4\pi^3}\int_{-\infty}^{\infty}d^2k_\parallel\int_{-\infty}^{\infty}\frac{d\omega}{\omega^2}\sum_{n=1}^{3}\Lambda_{ij}^{(n)}\times\exp\{i(\mathbf{k}_\parallel.\mathbf{x}_\parallel+k_3^{(n)}x_3-\omega t)\}, \tag{15}$$

where

$$\Lambda_{ij}^{(n)}=\frac{\mathrm{adj}(\mathbf{B})_j^{(n)}U_i^{(n)}}{\det|\mathbf{B}|}. \tag{16}$$

Since $G_{ij}^{\epsilon}(\mathbf{x},t)$ is real, it follows that its temporal Fourier transform has the property $\tilde{G}_{ij}^{\epsilon *}(\mathbf{x},\omega)=\tilde{G}_{ij}^{\epsilon}(\mathbf{x},-\omega)$, where the asterisk denotes complex conjugation. We exploit this property to restrict the integration over ω in (15) to the interval $[0,\infty]$, retaining only the real part. On further replacing the integration variable $\mathbf{k}_\parallel$ by $\mathbf{s}_\parallel=\mathbf{k}_\parallel/\omega$ we arrive at the result

$$G_{ij}^{\epsilon}(\mathbf{x},t)=-\frac{1}{2\pi^3}\mathrm{Re}\int_{-\infty}^{\infty}d^2s_\parallel\int_0^{\infty}d\omega\sum_{n=1}^{3}\Lambda_{ij}^{(n)} \times\exp\{i\omega(\mathbf{s}_\parallel\cdot\mathbf{x}_\parallel+s_3^{(n)}x_3-t)\}. \tag{17}$$

We treat the surface response and the response at interior points separately below.

II. SURFACE RESPONSE

By choosing the coordinate system suitably one can, without loss of generality, take the observation point $\mathbf{x}$ to be along the x_1 axis on the surface. Setting $x_2=x_3=0$, Eq. (17) simplifies to

$$G_{ij}^{\epsilon}(x_1,t)=-\frac{1}{2\pi^3}\mathrm{Re}\int_{-\infty}^{\infty}ds_1\int_0^{\infty}d\omega\Phi_{ij}(s_1) \times\exp\{i\omega(s_1x_1-t)\}, \tag{18}$$

where

$$\Phi_{ij}(s_1)=\int_{-\infty}^{\infty}ds_2\Psi_{ij}(\mathbf{s}_\parallel), \tag{19}$$

and

$$\Psi_{ij}(\mathbf{s}_\parallel)=\sum_{n=1}^{3}\Lambda_{ij}^{(n)}(\mathbf{s}_\parallel). \tag{20}$$

Convergence of the integral over ω is achieved by the replacement $(s_1x_1-t)\rightarrow(s_1x_1-t+i0_+)$. On integrating, one obtains

$$G_{ij}^{\epsilon}(x_1,t)=-\frac{1}{2\pi^3}\mathrm{Re}\int_{-\infty}^{+\infty}ds_1\frac{i\Phi_{ij}(s_1)}{(s_1x_1-t+i0_+)} =-\frac{1}{2\pi^3}\left[-\mathscr{P}\int_{-\infty}^{+\infty}ds_1\frac{\mathrm{Im}\ \Phi_{ij}(s_1)}{(s_1x_1-t)} +\frac{\pi}{|x_1|}\mathrm{Re}\ \Phi_{ij}(t/x_1)\right], \tag{21}$$

with $\mathscr{P}\int$ denoting the principal value of the integral.

Using the fact that for negative times $G_{ij}^{\epsilon}(x_1,t)$ is constant, and setting $G_{ij}^{\epsilon}(-x_1,-t)=G_{ij}^{\epsilon}(-x_1,0)$, $t>0$, we arrive at the Kramers–Kronig-type relation

$$-\mathscr{P}\int_{-\infty}^{+\infty}ds_1\frac{\mathrm{Im}\ \Phi_{ij}(s_1)}{s_1x_1-t}=\frac{\pi}{|x_1|}\mathrm{Re}\ \Phi_{ij}(t/x_1) +2\pi^3G_{ij}^{\epsilon}(-x_1,0). \tag{22}$$

It follows immediately from Eqs. (4), (21), and (22) that the response function pertaining to a Heaviside force is given by

$$G_{ij}^{\Theta}(x_1,t>0)=-\frac{1}{2\pi^2|x_1|}\mathrm{Re}\{\Phi_{ij}(t/x_1)-\Phi_{ij}(0)\}, \tag{23}$$

which, bearing in mind (19), is in the form of a one-dimensional integral. For an isotropic solid this integral can be evaluated analytically, but for an anisotropic solid, numerical methods are in general required for its evaluation.

A. Some properties of $\Psi_{ij}(\mathbf{s}_\parallel)$, $\Phi_{ij}(s_1)$, and $G_{ij}^{\Theta}(x_1,t)$

For small values of $\mathbf{s}_\parallel$ lying in the fully supersonic region enclosed by the curve of critical longitudinal (L) slownesses in the surface, all $s_3^{(n)}(\mathbf{s}_\parallel)$ are real, and hence $\Psi_{ij}(\mathbf{s}_\parallel)$ is real. Outside this critical curve, some or all of the $s_3^{(n)}\times(\mathbf{s}_\parallel)$ are complex or pure imaginary, and $\Psi_{ij}(\mathbf{s}_\parallel)$ is in general complex.

Further restrictions are imposed by the presence of materials symmetry. In the case where the x_3 axis lies along a twofold axis or is perpendicular to a symmetry plane, the following conditions hold:

The individual components of Ψ_{ij} are either symmetric or antisymmetric with respect to reversal of the direction of $\mathbf{s}_\parallel$:

$$\begin{aligned}&\Psi_{ij}(-\mathbf{s}_\parallel)=\Psi_{ij}(\mathbf{s}_\parallel),\quad ij\in(11,22,33,12,21),\\&\Psi_{ij}(-\mathbf{s}_\parallel)=-\Psi_{ij}(\mathbf{s}_\parallel),\quad ij\in(13,23,31,32).\end{aligned} \tag{24}$$

Likewise, for reversal of the direction of x_1,

$$\begin{aligned}&G_{ij}^{\Theta}(-x_1,t)=G_{ij}^{\Theta}(x_1,t),\quad ij\in(11,22,33,12,21),\\&G_{ij}^{\Theta}(-x_1,t)=-G_{ij}^{\Theta}(x_1,t),\quad ij\in(13,23,31,32).\end{aligned} \tag{25}$$

For large $\mathbf{s}_\parallel$ lying in the subsonic region outside the curve of limiting slow transverse (ST) slownesses, or transonic state as it is called, the solutions of Eq. (10), which takes the form of a cubic in s_3^2 because of symmetry, are all of the form $\pm iq$ or $\pm(p\pm iq)$, p,q real. The three discarded solutions are consequently $-s_3^{(n)}=s_3^{(n)*}$, where $s_3^{(n)}$ are the three chosen solutions corresponding to outgoing waves. It follows that

$$\Psi_{ij}(\mathbf{s}_\parallel,-s_3(\mathbf{s}_\parallel))=\Psi_{ij}^{*}(\mathbf{s}_\parallel,s_3(\mathbf{s}_\parallel)). \tag{26}$$

It is evident from Eqs. (9), (10), (12), (17), and (20) that

$$\Psi_{ij}(-\mathbf{s}_\parallel,-s_3(\mathbf{s}_\parallel))=-\Psi_{ij}(\mathbf{s}_\parallel,s_3(\mathbf{s}_\parallel)), \tag{27}$$

at all points except where $B_i^{(n)}$ is singular. From Eqs. (24), (25), and (26) one thus infers that, in the subsonic region away from singular points,

$$\begin{aligned}&\Psi_{ij}^{*}(\mathbf{s}_\parallel)=-\Psi_{ij}(\mathbf{s}_\parallel)\quad\text{and}\quad\Psi_{ij}(\mathbf{s}_\parallel)\ \text{is pure imaginary},\\&\qquad ij\in(11,22,33,12,21),\\&\Psi_{ij}^{*}(\mathbf{s}_\parallel)=\Psi_{ij}(\mathbf{s}_\parallel)\quad\text{and}\quad\Psi_{ij}(\mathbf{s}_\parallel)\ \text{is real},\\&\qquad ij\in(13,23,31,32).\end{aligned} \tag{28}$$

In the subsonic region, for all except possibly a few isolated directions of $\mathbf{s}_\parallel$, there is a single Rayleigh surface wave (RW) corresponding to the vanishing of $\det|B(\mathbf{s}_\parallel)|$ (see

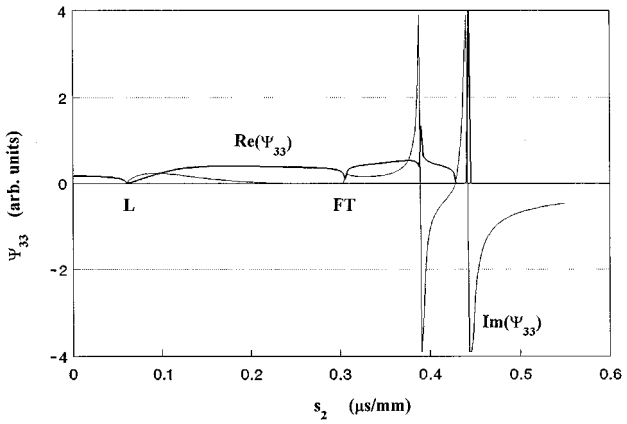

FIG. 1. $\Psi_{33}(s_1=0.21\mu s/\text{mm}, s_2)$ for the (001) surface of copper. Constants for the calculation are $C_{11}=169.0$, $C_{12}=122.0$, and $C_{44}=75.3$ in GPa, and $\rho=8960$ kg/m^3.

Ref. 35). This gives rise, for a given direction, to a simple pole in $\Psi_{ij}(s_\parallel)$ at s_R, which on being moved above the real axis yields, for $s_\parallel$ near s_R,

$$\Psi_{ij}(s_\parallel)\sim \mathrm{Res}_{s=s_R}\Psi_{ij}(s_\parallel)\left\{\mathscr{P}\left(\frac{1}{s_\parallel-s_R}\right)+i\pi\delta(s_\parallel-s_R)\right\}, \tag{29}$$

where $\mathrm{Res}_{s=s_R}\Psi_{ij}(s_\parallel)$ denotes the residue of $\Psi_{ij}(s_\parallel)$ at $s_\parallel=s_R$. Hence for $s_\parallel$ near s_R,

$$\begin{aligned}&\mathrm{Re}(\Psi_{ij}(s_\parallel))\sim i\pi[\mathrm{Res}_{s=s_R}\Psi_{ij}(s_\parallel)]\delta(s_\parallel-s_R),\\ &\qquad ij\in(11,22,33,12,21),\\ &\mathrm{Re}(\Psi_{ij}(s_\parallel))\sim[\mathrm{Res}_{s=s_R}\Psi_{ij}(s_\parallel)]\mathscr{P}\left(\frac{1}{s_\parallel-s_R}\right),\\ &\qquad ij\in(13,23,31,32).\end{aligned} \tag{30}$$

For large s_1, beyond where the line $s_1=$constant intersects the RW slowness curve,

$$\mathrm{Re}(\Psi_{ij}(\mathbf{s}_\parallel))=0,\ \ (\Phi_{ij}(s_1))=0 \tag{31}$$

and

$$G^{\Theta}_{ij}(x_1,t)=\frac{\Phi_{ij}(0)}{2\pi^2|x_1|}=\text{const}$$

$$\text{for } ij\in(11,22,33,12,21).$$

If, further, the (x_1,x_3) plane is a materials symmetry plane, then

$$G^{\Theta}_{ij}(x_1,t)\equiv 0 \quad \text{for } ij\in(32,23,21,12). \tag{32}$$

B. Numerical integration and results

For an anisotropic solid the integration over s_2 in (19) to obtain Φ_{ij} has, in general, to be done numerically, and the method of integration has to cope with the RW poles and, in cases where they exist, pseudo-surface-acoustic-wave (PSAW) resonances.[34] This point is brought out in Fig. 1, which shows the dependence of Ψ_{33} on s_2 for fixed $s_1=0.21$ μs/mm for the (001) surface of copper. The reference

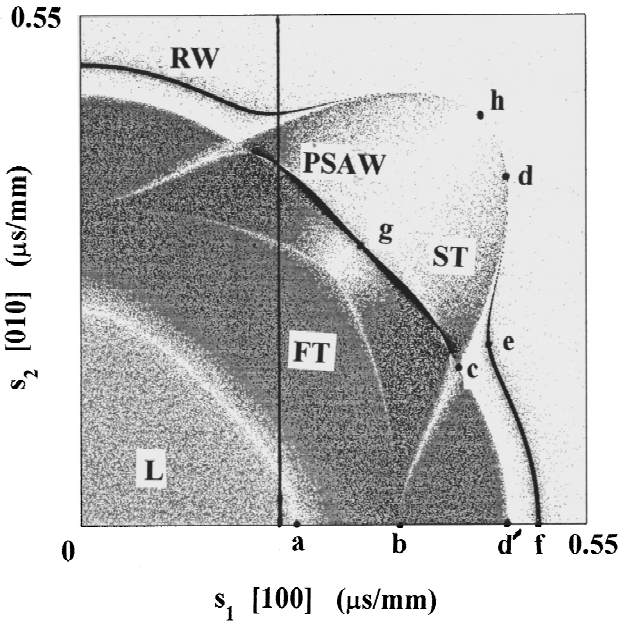

FIG. 2. Gray-scale representation of $\mathrm{Re}(\Psi_{33}(s_1,s_2))$ for Cu(001).

axes are aligned along the principal crystallographic directions, and Ψ_{33} is unchanged by a reversal in the sign of s_1 or s_2. The real part of Ψ_{33} displays a sharp peak at 0.39 μs/mm, which is associated with a PSAW resonance. For $s_2>0.43$ μs/mm, Ψ_{33} is pure imaginary except for a δ-function singularity at 0.45 μs/mm, associated with the RW pole. Sharp dips occur in $\mathrm{Re}(\Psi_{33})$ at the limiting L and one of the limiting fast transverse (FT) slownesses.

A global picture is provided by Fig. 2, which portrays the dependence of $\mathrm{Re}(\Psi_{33})$ on both s_1 and s_2 as a gray-scale ''image,'' with degree of darkness corresponding to the magnitude of $\mathrm{Re}(\Psi_{33})$. To render the RW singularity visible, it has been artificially broadened by making the replacement

$$\Psi_{33}\rightarrow 1/(1/\Psi_{33}+\alpha), \tag{33}$$

where α is a small but finite positive number. A similar effect can be achieved by ascribing a small imaginary part to $\mathbf{s}_\parallel$. The vertical line in this image represents the ''line scan'' for the data in Fig. 1. The continuously shaded area in Fig. 2 comprises the Ψ_{33} weighted projections $\mathbf{s}_\parallel$ of the slowness vectors of all bulk modes in the first quadrant, its outer boundary being the so-called transonic state. The lines which stand out as lighter and which partition this domain, lie on the locus of limiting slownesses. This locus and the transonic state are the projection on the (s_1,s_2) plane of points on the three sheets of the slowness surface where the surface normal is parallel to the (s_1,s_2) plane. Along the [110] direction, the diagonal in Fig. 2, the ST bulk modes are SH polarized normal to the $(\bar{1}10)$ symmetry plane, and thus do not contribute to $\mathrm{Re}(\Psi_{33})$, as is evident from the fading of the ST modes in this region. The sharp RW resonance is most intense in the $\langle 100\rangle$ directions, and fades away towards the [110] direction, where it degenerates with the transonic state.

In the region extending about 20° to either side of the [110] direction there is a PSAW resonance lying within the band of ST bulk modes. Exactly in the [110] direction where

the RW degenerates, the PSAW becomes a pure supersonic two component surface acoustic wave (SAW).

The method we have used in calculating $G_{ij}^{\Theta}(x_1,t)$, is to make the replacement (33) and then evaluate the integral (19) numerically for 250 values of t. This is consistent in spirit with the numerical approach to inversion taken by a number of authors (see Ref. 7 and papers cited therein). Over most of the range of s_2, Ψ_{ij} is slowly varying, but in isolated regions there are the sharp RW and PSAW resonances, and kinks at limiting branch slownesses to contend with. We have dealt with this problem by dividing the range of s_2 into a number of intervals, a thousand is more than sufficient, and applying Rhomberg integration to each interval. It is only the few intervals where Ψ_{ij} is rapidly varying that more than one Rhomberg iteration is required to achieve convergence.

The above method has the advantage of simplicity and generality. With the coding we have implemented, it takes in the region of 15 min on a 133-MHz pentium personal computer to generate surface response functions of the type displayed in this paper, but this time can be considerably reduced at the cost of rounding of the sharp features. For instance, the response function for the fiber composite in Fig. 1 of Tewary and Fortunko[14] can be reproduced in less than one minute, or less still if fewer than 250 values of t are taken. Bearing in mind that our coding has been set up for general anisotropy, whereas that of Ref. 14 is specialized to tetragonal symmetry, it appears that their and our algorithms are comparable in numerical efficiency.

C. Wave arrival singularities

Figure 3(a) shows the surface response function $G_{33}^{\Theta}(x_1=100\ \text{mm}, x_2=0, t)$ calculated for the (001) surface of copper. The response is zero until $t_a=23.1\ \mu$s, at which moment there is a sudden downward kink corresponding to a discontinuous change in velocity. This event is associated with the sharp dip in $\text{Re}(\Psi_{33})$ at the limiting longitudinal slowness labeled *a* in Fig. 2, which is a branch point in the complex function Ψ_{33}. The kinks in G_{33}^{Θ} at $t_b=34.4\ \mu$s and $t_c=40.2\ \mu$s correspond to the limiting transverse slownesses labeled *b* and *c* in Fig. 2. These are bulk wave arrival singularities, and correspond to points on the slowness surface where the normal points in the observation direction. These singularities propagate outwards from the point of excitation at the bulk wave group velocities in that direction. Bulk wave singularities and the analytic form they take in the response functions of infinite anisotropic continua have been surveyed in Ref. 1. It is evident that a surface response function must also show nonanalytic behavior as the integration path $s_1=\text{const}$ makes tangential contact with a limiting slowness curve, since to one side it has a double intersection with this curve, which is a locus of branch points, while on the other side it has no intersection.

At the surface there are also RW wave arrival singularities. These are generally much more prominent than the bulk wave arrivals, and so we devote more attention to them here. RW arrivals are conditioned by tangency of the line $s_1=s_R=t_R/|x_1|$ to the RW slowness curve. At the point of tangency the RW group velocity, which is normal to the RW

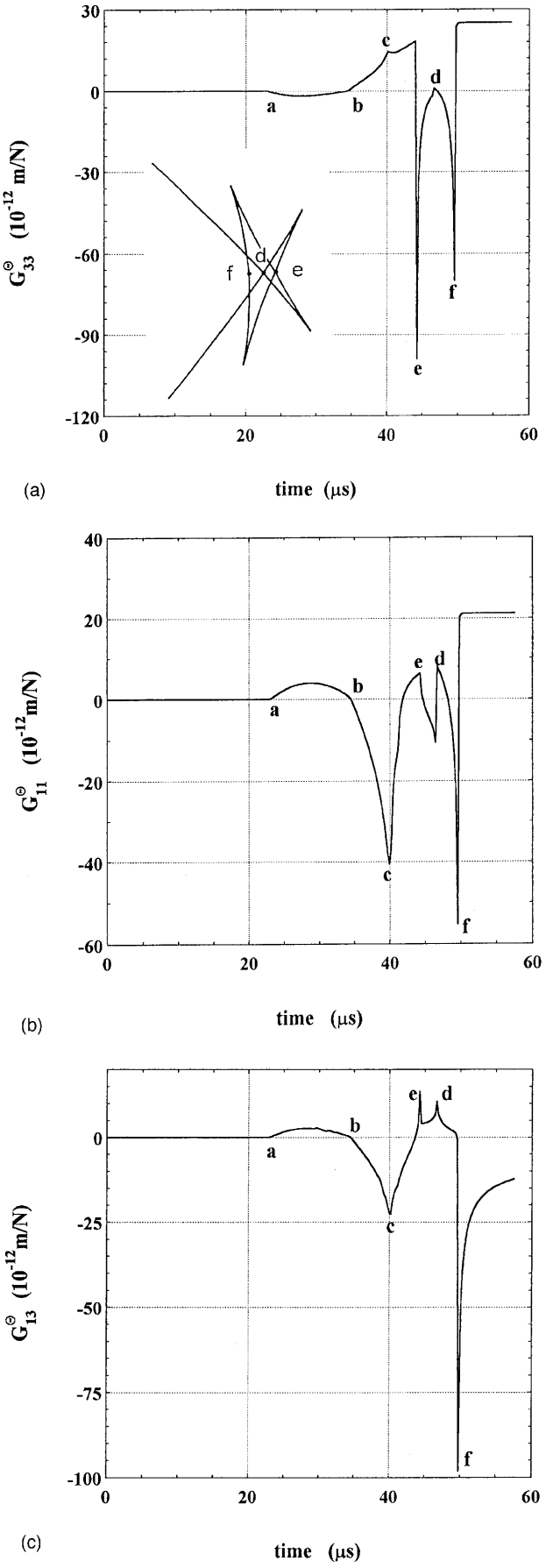

FIG. 3. Surface responses G_{ij}^{Θ} ($x_1=100$ mm, $x_2=x_3=0,t$) for Cu(001). (a) G_{33}^{Θ}, (b) G_{11}^{Θ}, (c) G_{13}^{Θ}. The insert in (a) shows a portion of the RW group velocity curve near the ⟨100⟩ direction.

slowness curve and hence parallel to the x_1 axis, is of magnitude $1/s_R$, and this is the velocity with which the wave arrival singularity propagates along the surface. The analytical form of G_{ij}^{Θ} for t near t_R depends on whether the surface of the half-space is a materials symmetry plane or not, and if it is, whether $ij \in (11,22,33,12,21)$ or $ij \in (13,23,31,32)$, and finally whether the RW slowness curve is convex or concave at the point of tangency.

Taking the surface to be a materials symmetry plane, $ij \in (11,22,33,12,21)$, and the RW slowness curve to be convex, then for $t<t_R$ the line $s_1=t/|x_1|$ intersects the RW slowness curve twice near the point of tangency. In this region, the RW slowness is, in the parabolic approximation with the origin for s_2 located at the point of tangency, given by $s_1=s_R-\beta s_2^2$, where β is the (positive) curvature. From Eqs. (19), (23), and (30) the singular part of G_{ij}^{Θ} thus takes the form

$$G_{ij}^{\Theta}(x_1,t)=\frac{A}{2\pi|x_1|}\int_{-\infty}^{\infty} ds_2\ \delta\left(\beta s_2^2-\left[\frac{t_R-t}{|x_1|}\right]\right), \tag{34}$$

where $A=-\,i\ \mathrm{Res}_{s=s_R}\Psi_{ij}$ is a real constant for the purpose of the integration (although it does depend on the direction of x_1). The integral is readily evaluated, yielding

$$G_{ij}^{\Theta}(x_1,t)=\frac{A}{2\pi|x_1|^{1/2}\beta^{1/2}(t_R-t)^{1/2}}. \tag{35}$$

For $t>t_R$, $\Psi_{ij}=0$ in the region of tangency, and so the integral vanishes and G_{ij}^{Θ} is given by the constant term in Eq. (23). The wave arrival is thus led by an inverse square-root divergence and terminated by an infinite discontinuity. It may happen that there are other intersections of the line $s=s_R$ with the closed RW slowness curve, in which case there is a background in the neighborhood of t_R, which varies linearly with t, but after the last intersection, G_{ij}^{Θ} is exactly constant.

If at the point of tangency the RW slowness curve is concave, then the wave arrival is initiated by an infinite discontinuity, after which G_{ij}^{Θ} varies as $(t-t_R)^{-1/2}$.

For $ij \in (13,23,31,32)$ and the RW slowness curve concave, reference to Eqs. (19), (23), and (30) shows that the singular part of G_{ij}^{Θ} takes the form

$$G_{ij}^{\Theta}(x_1,t)=\frac{A}{2\pi^2|x_1|}\mathscr{P}\int_{-\infty}^{\infty}\frac{ds_2}{\left(\beta s_2^2+\left[\frac{t_R-t}{|x_1|}\right]\right)}. \tag{36}$$

On integrating, for $t<t_R$ this yields Eq. (35). For $t>t_R$ the path of integration intersects the RW slowness curve twice, and on taking the principal part of the integral, the result is zero, so that G_{ij}^{Θ} is constant. When the RW slowness curve is convex, these conditions are reversed, and the divergence follows the RW arrival.

In summary:

$$G_{ij}^{\Theta}(x_1,t)=\begin{cases}\dfrac{A_<}{2\pi|x_1|^{1/2}\beta^{1/2}(t_R-t)^{1/2}}, & t<t_R\\[2ex] \dfrac{A_>}{2\pi^2|x_1|}, & t>t_R,\end{cases} \tag{37}$$

for $ij \in (11,22,33,12,21)$, RW slowness curve convex,

$ij \in (13,23,31,32)$, RW slowness curve convcave,

where $A_>$ and $A_<$ are constants, and

$$G_{ij}^{\Theta}(x_1,t)=\begin{cases}\dfrac{A_<}{2\pi^2|x_1|}, & t<t_R\\[2ex] \dfrac{A_>}{2\pi|x_1|^{1/2}\beta^{1/2}(t-t_R)^{1/2}}, & t>t_R,\end{cases} \tag{38}$$

for $ij \in (11,22,33,12,21)$, RW slowness curve concave,

$ij \in (13,23,31,32)$, RW slowness curve convex.

The singular behavior displayed by the analytical solutions for isotropic solids[27,28] conforms to the above rules.

In the situation where the surface is not a materials symmetry plane, $\mathrm{Re}\, s_{s=s_R}\Psi_{ij}$ has both real and imaginary parts for all ij, and it follows that G_{ij}^{Θ} diverges on both sides of the RW arrival in accordance with

$$G_{ij}^{\Theta}(x_1,t)=\frac{A_{\gtrless}}{2\pi|x_1|^{1/2}|\beta|^{1/2}|t_R-t|^{1/2}}. \tag{39}$$

The above results are consistent with Willis'[32] treatment of RW arrival singularities.

In anisotropic solids the displacement leading or trailing the RW arrival can vary enormously with direction. One source of this variation is the factor A. In directions for which the plane of polarization of the RW is perpendicular to the i or j axis, A is zero. For all ij, A also vanishes at points where the RW degenerates with the transonic state, as is evident in Fig. 2.

A second source of variation is that the singular part of the waveform is proportional to $|\beta|^{-1/2}$, and hence the wave intensity is proportional to $|\beta|^{-1}$. Variation in intensity through the curvature of the RW slowness curve in this way is known as surface phonon focusing, and has been studied theoretically by a number of authors.[36–39] The effects have been observed experimentally with laser generated ultrasonic SAW[18] and ballistic surface phonons.[40]

At points of inflection where $\beta=0$, the parabolic approximation for the RW slowness equation breaks down. Taking x_1 and s_1 in the direction of the normal to the RW slowness curve at the point of inflection, the RW slowness equation to leading order now takes the form $s_1=s_R-\gamma s_2^3$, $\gamma=$ constant. On integrating over s_2, one readily establishes that the singular part of G_{ij}^{Θ} near the wave arrival has the form

$$G_{ij}^{\Theta}(x_1,t)=\frac{A_{\gtrless}}{6\pi|x_1|^{1/3}|\gamma|^{1/3}|t_R-t|^{2/3}}. \tag{40}$$

The inverse square-root dependence on x_1 and β for normal points, and the inverse third power dependence on x_1 and γ for points of inflection, is a characteristic also of frequency domain surface Green's functions in the asymptotic far-field limit.[36,38,39]

If the direction of the x_1 axis is changed slightly, then for one sense of rotation there are now two values of s_1 at which tangency occurs, and thus two wave arrivals propagating at slightly different group velocities. For the opposite sense of rotation there are no longer any points of tangency near the inflection point, and so no wave arrivals. It follows thereby that the point of inflection maps onto a cusp in the group velocity curve. Criteria for the existence of cusps in respect of the (100) and (111) surfaces of cubic crystals have been established by Maznev and Every.[41] Extending some distance beyond the cusp, where there is no longer any wave arrival in the strict sense, is a quasisingular feature which we refer to as an eidolon.[42] It has been observed for laser generated SAW by Maznev *et al.*[43]

Referring again to Fig. 3(a), the sharp dip at $t_e = 44.3$ μs is a RW singularity having the analytic form (38). The curvature of the RW slowness curve near point e is negative in this case, and so the RW arrival is manifested as a sudden dip followed by an initially steep continuous rise. The sharp dip at $t_f = 49.5$ μs is a RW singularity having the analytic form (37). It is shaped the familiar way around as encountered in the response function G_{33}^{Θ} of isotropic solids, because in this case the RW slowness curve near f is convex. Beyond t_f, G_{33}^{Θ} is constant, because $\mathrm{Re}(\Psi_{33})$ is zero. There is a third RW singularity of the form (37) at t_d, but it shows up very faintly in the calculated response because, as can be seen in Fig. 2, point d is very close to where the RW degenerates with the transonic state and becomes SH in character. It also occurs very close to the transonic state d', and it is difficult to distinguish the two features from each other in this plot. The inset in Fig. 3(a) shows the folded character of the RW group velocity curve for Cu(001) near the x_1 axis. The three aforementioned wave arrivals correspond to the three points where the x_1 axis intersects this curve.

Figure 4 is a gray-scale representation of the dependence of $\mathrm{Re}(\Psi_{11})$ on s_1 and s_2. Since Ψ_{11} selects out the s_1 axis, this plot does not display mirror symmetry across the diagonal (reflecting Ψ_{11} across the diagonal in fact yields Ψ_{22}). In the region of the s_1 axis $\mathrm{Re}(\Psi_{11})$ shows a prominent peak at the L threshold (point a), rather than the dip as in the case of $\mathrm{Re}(\Psi_{33})$. This quasisurface L mode resonance has been reported on before, and shows up in phonon imaging,[44–46] surface Brillouin scattering[47,48] and elsewhere. Towards the s_2 axis this resonance disappears (point b) because the L mode is polarized normal to the s_1 axis and so does not contribute to $\mathrm{Re}(\Psi_{11})$. Here the L mode resonance is at a maximum in $\mathrm{Re}(\Psi_{22})$. The RW, which is composed of inhomogeneous waves of predominantly L and T character, shows similar behavior to the L resonance, being most intense near the s_1 axis and fading to zero towards the s_2 axis.

Figure 3(b) shows the surface response function $G_{11}^{\Theta}(x_1 = 100 \text{ mm}, x_2, t)$ for Cu(001). As can be seen, the L bulk wave arrival is much more pronounced than for G_{33}^{Θ}, and the same applies to the bulk wave feature c, which can be understood by reference to Fig. 4. The RW singularities are the same way around as for G_{33}^{Θ}, except that in this case feature d is more pronounced and e much less so, which can be understood by reference to Fig. 4.

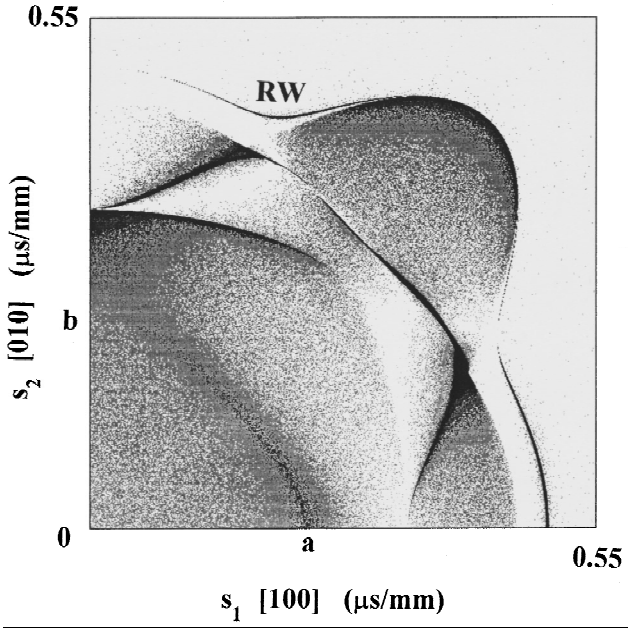

FIG. 4. Gray-scale representation of $\mathrm{Re}(\Psi_{11}(s_1, s_2))$ for Cu(001).

Figure 3(c) shows the response function $G_{13}^{\Theta}(x_1 = 100 \text{ mm}, x_2, t)$ for Cu(001). One notes that in this case it is the wave arrival e that is of type (37), and the wave arrival f that is of type (38), so that after this last wave arrival there is a smooth asymptotic approach to the static response. Because the (x_1, x_3) plane is a crystallographic symmetry plane for Cu(001), $G_{ij}^{\Theta}(x_1, t) = 0$ for $ij \in 12,21,32,23$.

III. INTERIOR RESPONSE

Without loss of generality, we locate the observation point in the (x_1, x_3) plane. In the case of homogeneous waves corresponding to real $s_3^{(n)}$, convergence of the integral over ω in Eq. (16) is achieved through the replacement $(s_1 x_1 + s_3^{(n)} x_3 - t) \rightarrow (s_1 x_1 + s_3^{(n)} x_3 - t + i0_+)$. For inhomogeneous waves, $s_3^{(n)} x_3$ already comprises a positive imaginary part, and convergence is assured without the abovementioned replacement. On integrating over ω we obtain

$$G_{ij}^{\epsilon}(\mathbf{x}, t) = -\frac{1}{2\pi^3 |\mathbf{x}|} \mathrm{Re} \int_{-\infty}^{\infty} d^2 s_{\parallel} \times \sum_{n=1}^{3} \frac{i \Lambda_{ij}^{(n)}(\mathbf{s}_{\parallel})}{s_1 \sin\theta + s_3^{(n)} \cos\theta - t/|\mathbf{x}| + i0_+}, \quad (41)$$

where $\tan\theta = x_1/x_3$. Essentially the same result is to be found in Willis[32] and in Wang and Achenbach,[4] except that they transform to radial and angular coordinates for $\mathbf{s}_{\parallel}$.

A. Numerical integration

To obtain the full time dependence of $G_{ij}(\mathbf{x}, t)$ at a given point $\mathbf{x}$, $s_3^{(n)}$ and $\Lambda_{ij}^{(n)}$ have to be determined for a two-dimensional (2D) manifold of points $\mathbf{s}_{\parallel}$. Discretization

for numerical purposes reduces this to calculating $s_3^{(n)}$ and $\Lambda_{ij}^{(n)}$ at say $\sim 10^3 \times 10^3 = 10^6$ points $\mathbf{s}_\parallel$, depending on the required accuracy. Treating (41) in a simpleminded way as a summation to obtain $G_{ij}(\mathbf{x},t)$ for say 240 values of t, involves an additional $240 \times 3 \times 10^6 \approx 10^9$ calculations, which in our experience, takes almost twice as long as the calculating of $s_3^{(n)}$ and $\Lambda_{ij}^{(n)}$. This is an unacceptable computational overhead. This problem has long been recognized, and sophisticated methods have been proposed for overcoming it. The Cagniard–de Hoop[5] method and the method developed by Willis[32] and Wang and Achenbach,[4] all reduce the evaluation of $G_{ij}(\mathbf{x},t)$ to a one-dimensional (1-D) angular integral, in which the integrand has to be determined iteratively for each value of t. The latter authors accomplish this by changing to radial and angular coordinates for $\mathbf{s}_\parallel$ and evaluating the integral over $|\mathbf{s}_\parallel|$ using the Cauchy residue theorem. This requires finding all the zeros in the complex plane of the denominator in (41) and determining the derivative of this denominator with respect to $|\mathbf{s}_\parallel|$. Information about $\Lambda_{ij}^{(n)}$ over the 2-D manifold is still required, but the overhead is considerably reduced. The Cagniard–de Hoop method has been widely applied to isotropic and transversely isotropic solids,[33] but only recently has it been implemented computationally to a significant extent for anisotropic solids.[5]

We have adopted the following numerical scheme for calculating $G_{ij}(\mathbf{x},t)$, which is much simpler than the above-mentioned methods, but which nevertheless, like them, substantially reduces the computational overhead. We proceed by casting (41) in the form

$$G_{ij}^{\epsilon}(\mathbf{x},t) = -\frac{1}{2\pi^3|\mathbf{x}|}\mathrm{Re}\left\{\int_{-\infty}^{\infty}\frac{f_{ij}(u)du}{u - t/|\mathbf{x}| + i0_+} + \int_{-\infty}^{\infty}du\int_0^{\infty}\frac{g_{ij}(u,v)dv}{u+iv-t/|\mathbf{x}|}\right\}, \tag{42}$$

where the auxiliary functions $f_{ij}(u)$ and $g_{ij}(u,v)$ are given by

$$f_{ij}(u) = \sum_{n=1}^{3}\int_{\Omega_n} d^2 s_\parallel \delta(u - \mathrm{Re}[s_1 \sin\theta + s_3^{(n)}\cos\theta]) i\Lambda_{ij}^{(n)}, \tag{43}$$

$$g_{ij}(u,v) = \sum_{n=1}^{3}\int_{\Omega_n'} d^2 s_\parallel \delta(u - \mathrm{Re}[s_1 \sin\theta + s_3^{(n)}\cos\theta])\,\delta(v - \mathrm{Im}[s_3^{(n)}\cos\theta]) i\Lambda_{ij}^{(n)}, \tag{44}$$

where Ω_n and Ω_n' are the domains in the (s_1, s_2) plane in which $s_3^{(n)}$ is real and complex, respectively.

All the detailed structure of $G_{ij}(\mathbf{x},t)$ is derived from $f_{ij}(u)$, while $g_{ij}(u,v)$, which tends linearly with v to zero towards the axis $v=0$, provides merely a smooth continuous background. For numerical purposes we divide the line u into a large number (7680) of intervals, and generate $f_{ij}(u)$ as a histogram of the accumulated values of $i\Lambda_{ij}^{(n)}$ for each interval in accordance with (43). The 1-D integral in (42), evaluated for 240 values of t thereby involves $\sim 1.8 \times 10^6$ calculations. In performing the 2-D integral, we divide the upper half of the (u,v) plane into a course grid of 240×120 cells, and generate a 2-D histogram in accordance with (44), and then carry out the sum for the 240 values of t, which involves $\sim 6.9 \times 10^6$ calculations. The overhead is reduced in this way by more than a factor of 10 to less than 20% of the total computational time, which is acceptable. The computational time for the interior response functions presented below is under 15 min, which is less than that required to generate the surface response functions provided earlier, which nominally involve only 1-D numerical integration. The coding was kept general, with no advantage taken of symmetry other than taking the sample surface to be a materials symmetry plane to render Eq. (10) cubic in s_3^2.

It is appropriate at this point to comment on the relative merits and disadvantages of the contour integration methods mentioned earlier, as compared with the numerical approach described above. One could argue that, as a matter of principle, it is better to do as many integrations analytically as possible and only resort to numerical integration as a last resort. It might also be argued that integrals over a finite domain, as in Wang and Achenbach,[4] are more amenable to evaluation than the infinite integrals in our approach. Successful implementation of the method of Wang and Achenbach for a point force would, however, require the use of a robust and efficient algorithm for locating the poles in the complex plane, and for keeping track of the branch points and Riemann cuts. These calculations would have to be embedded in loops for varying t and the angular coordinate ϕ of $\mathbf{s}$. Divergences of the integrand in the integration over ϕ would have to be accommodated. We would anticipate that it is nevertheless possible to achieve greater numerical efficiency in this way, but at the cost of increased complexity in the coding. In progressing onto more complicated systems such as joined anisotropic half spaces and layered solids the problems will be more acute, and there may be a clear advantage to adopting a simple numerical approach of the type we have introduced here.

B. Results

Figure 5(a) shows calculated half-space response functions G_{33}^{Θ} for hexagonal zinc, with the surface of the half-space normal to the principal crystallographic axis. Three observation points have been chosen, namely $x_1 = 0$, 5, and 10 mm, with $x_3 = 25.8$ mm, partly for comparison with published experimental data.[7] These display a number of bulk wave arrival singularities labeled L (a discontinuity), I (a logarithmic discontinuity), S (a discontinuity followed by a gradual rise and leveling off), X, and C. These wave arrivals correspond to intersections of the viewing direction with sheets of the wave surface of zinc as shown in Fig. 6. In the epicentral direction, $x_1 = 0$, the two quasi-T sheets I and S of the wave surface intersect at a conical point, and the response shows a negative square-root divergence, which is associated with the phenomenon of external conical refraction.[23,24] The intersection F leads to a kink and a discontinuity which are barely perceptible in the response. For $x_1 = 10$ mm the I and F wave arrivals coincide at C, at a

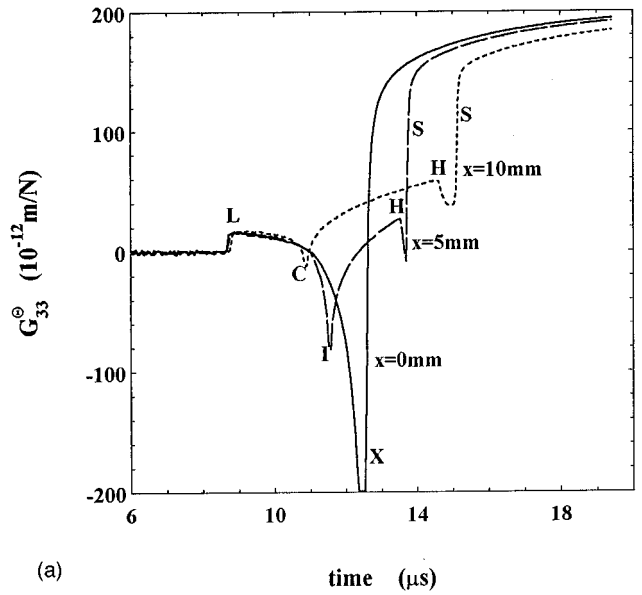

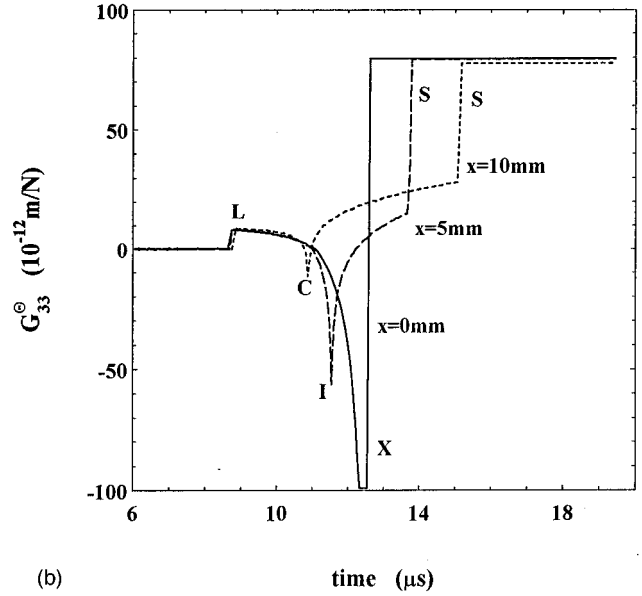

FIG. 5. (a) G_{33}^{Θ} ($x_1 = x, x_2 = 0, x_3 = 25.8$ mm) for a (0001)-oriented zinc semi-infinite continuum at interior points $x=0$ (epicenter), 5 mm, and 10 mm. Constants for the calculation are $C_{11}=163.75, C_{12}=36.28$, $C_{13}=52.48, C_{33}=62.93$, and $C_{44}=38.68$ in GPa, and $\rho=7140$ kg/m^3. (b) G_{33}^{Θ} for the same points in a zinc infinite continuum.

cuspidal edge of the wave surface. There are no prominent singular features associated with the pure-T sheet of the wave surface, which is therefore not shown in Fig. 6. Slightly preceding the S arrival is the head wave arrival H, whose geometrical relation to the wave surface is shown in Fig. 6. Zinc is somewhat unusual in that the head wave merges with the wave surface at a point very close to the conical point.[25] These calculated responses are in very good agreement with waveforms measured in zinc by Kim *et al.*,[49,50] particularly with regard to the bulk and head wave arrivals.

Figure 5(b) shows zinc infinite continuum response functions calculated for the same configurations as above using the method of Ref. 1. Overall the displacements are

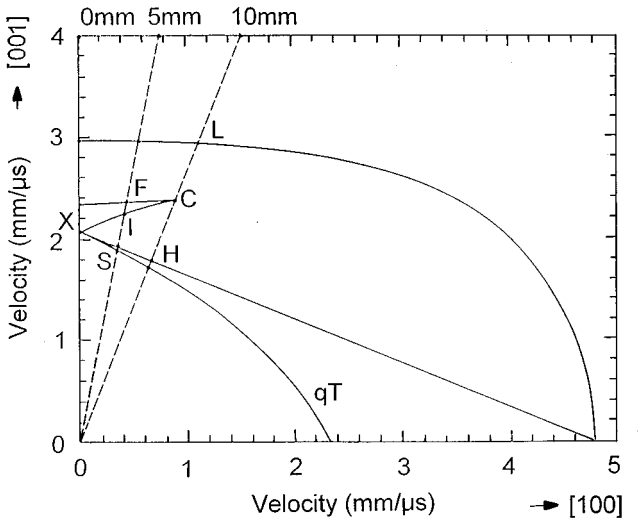

FIG. 6. Zonal section of the qL and qT sheets of the wave surface of zinc.

reduced in magnitude by about a factor of 2 as compared with those for the half-space, as one would expect. The bulk wave arrivals are of the same analytic form and occur at the same times as for the half-space. Head wave effects are of course absent from the infinite continuum results. Another difference is the constant displacement in the infinite continuum response following the last S arrival, as compared with the asymptotic leveling off in the half-space response.

IV. CONCLUSIONS

We have derived integral expressions for the surface and interior displacement response of a semi-infinite anisotropic elastic continuum subjected to sudden surface loading. By way of numerical example, calculated surface responses of Cu(001) and interior responses of Zn(0001) have been presented. The surface responses display bulk and surface wave arrival singularities, and the interior responses display bulk and head wave arrival singularities. In follow up papers we will use these methods in the interpretation of capillary fracture generated waveforms measured in a number of different materials.

[1] A. G. Every and K. Y. Kim, J. Acoust. Soc. Am. **95**, 2505 (1994).
[2] K. Y. Kim, A. G. Every, and W. Sachse, J. Acoust. Soc. Am. **95**, 1942 (1994).
[3] C. Y. Wang and J. D. Achenbach, Wave Motion **16**, 389 (1992); **18**, 273 (1993); Proc. R. Soc. London, Ser. A **449**, 441 (1995).
[4] C. Y. Wang and J. D. Achenbach, Wave Motion **24**, 227 (1996).
[5] A. Mourad and M. Deschamps, J. Acoust. Soc. Am. **97**, 3194 (1995); Acustica united with Acta Acustica **82**, 839 (1996).
[6] P. Borejko and S. K. Datta, Z. Angew. Math. Mech. **74**, T272 (1994).
[7] R. L. Weaver, W. Sachse, and K. Y. Kim, J. Appl. Mech. **63**, 337 (1996).
[8] H. Zhu, ASME J. Appl. Mech. **59**, S96 (1992).
[9] A. N. Norris, Proc. R. Soc. London, Ser. A **447**, 175 (1994).
[10] R. Burridge, P. Chadwick, and A. N. Norris, Proc. R. Soc. London, Ser. A **440**, 655 (1993).
[11] S. Tamura and M. Yagi, Phys. Rev. B **49**, 17378 (1994).
[12] V. K. Tewary and C. M. Fortunko, J. Acoust. Soc. Am. **91**, 1888 (1992).
[13] V. K. Tewary, Phys. Rev. B **51**, 15695 (1995).
[14] V. K. Tewary and C. M. Fortunko, J. Acoust. Soc. Am. **100**, 86 (1996).
[15] A. G. Every, W. Sachse, K. Y. Kim, and M. O. Thompson, Phys. Rev. Lett. **65**, 1446 (1990); A. G. Every and W. Sachse, Phys. Rev. B **44**, 6689 (1991).

[16] B. Castagnede and A. Mourad, C. R. Acad. Sci. Paris II **314**, 1301 (1992); II **316** (1993).
[17] J. F. Chai and T. T. Wu, J. Acoust. Soc. Am. **95**, 3232 (1994).
[18] Al. A. Kolomenskii and A. A. Maznev, Phys. Rev. B **48**, 14 502 (1993).
[19] R. L. Weaver, M. R. Hauser, and J. P. Wolfe, Z. Phys. B **90**, 27 (1993).
[20] R. E. Vines, S. Tamura, and J. P. Wolfe, Phys. Rev. Lett. **74**, 2729 (1995); R. E. Vines, M. R. Hauser, and J. P. Wolfe, Z. Phys. B **98**, 255 (1995).
[21] J. P. Wolfe and M. R. Hauser, Ann. Physik **4**, 99 (1995).
[22] J. Wesner, K. U. Würz, K. Hillmann, and W. Grill, in *Phonon Scattering in Condensed Matter VII*, edited by M. Meissner and R. O. Pohl (Springer-Verlag, Berlin, 1993), 68 pp.
[23] K. Y. Kim, W. Sachse, and A. G. Every, Phys. Rev. Lett. **70**, 3443 (1993).
[24] K. Y. Kim, A. G. Every, and W. Sachse, Int. J. Mod. Phys. B **8**, 2327 (1994).
[25] M. J. P. Musgrave and R. G. Payton, Q. J. Mech. Appl. Math. **34**, 235 (1982); **35**, 173 (1982).
[26] H. Lamb, Philos. Trans. R. Soc. London, Ser. A **203**, 1–42 (1904).
[27] J. D. Achenbach, *Wave Propagation in Elastic Solids* (North-Holland, Amsterdam, 1973).
[28] A. C. Eringen and E. S. Suhubi, *Elastodynamics* (Academic, New York, 1975).
[29] R. Burridge, Q. J. Mech. Appl. Math. **24**, 81 (1971).
[30] A. A. Maznev and A. G. Every, Int. J. Eng. Sci. **35**, 321 (1997).
[31] J. H. M. T. van der Hijden, *Propagation of Transient Elastic Waves in Stratified Anisotropic Media* (North-Holland, Amsterdam, 1987).
[32] J. R. Willis, Philos. Trans. R. Soc. London, Ser. A **274**, 435 (1973).
[33] R. G. Payton, *Elastic Wave Propagation in Transversely Isotropic Media* (Martinus Nijhoff, The Hague, 1983).
[34] G. W. Farnell, in *Physical Acoustics*, edited by W. P. Mason and R. N. Thurston (Academic, New York, 1970), Vol. VI, 109 pp.
[35] J. Lothe and D. M. Barnett, J. Appl. Phys. **47**, 428 (1976).
[36] H. Shirasaki and T. Makimoto, J. Appl. Phys. **49**, 658 (1978); **49**, 661 (1978); **50**, 2795 (1979).
[37] S. Tamura and K. Hongo, Jpn. J. Appl. Phys. **20**, Suppl. 20-3, 17 (1981).
[38] R. E. Camley and A. A. Maradudin, Phys. Rev. B **27**, 1959 (1983).
[39] L. A. Chernozatonskii and V. V. Novikov, Solid State Commun. **51**, 643 (1984).
[40] C. Höss and H. Kinder, Physica B **219&220**, 706 (1996).
[41] A. A. Maznev and A. G. Every, Acustica united with Acta Acustica **1**, 137 (1994); Solid State Commun. **97**, 679 (1996).
[42] K. Y. Kim, K. C. Bretz, A. G. Every, and W. Sachse, J. Appl. Phys. **79**, 1857 (1996).
[43] A. A. Maznev, A. A. Kolomenskii, and P. Hess, Phys. Rev. Lett. **75**, 332 (1995).
[44] A. G. Every, G. L. Koos, and J. P. Wolfe, Phys. Rev. B **29**, 2190 (1984).
[45] D. C. Hurley, A. G. Every, and J. P. Wolfe, J. Phys. C **17**, 3157 (1984).
[46] A. G. Every, Phys. Rev. B **33**, 2719 (1986).
[47] G. Carlotti, D. Fioretto, L. Giovanni, F. Nizzoli, G. Socino, and L. Verdini, J. Phys.: Condens. Matter **4**, 257 (1992).
[48] R. E. Camley and F. Nizzoli, J. Phys. C: Solid State Phys. **18**, 4795 (1985).
[49] K. Y. Kim and W. Sachse, J. Appl. Phys. **75**, 1435 (1994).
[50] K. Y. Kim, Wave Motion **20**, 83 (1994).